

First-principles study on the high-pressure phase transition and elasticity of KAlSi_3O_8 hollandite

KENJI KAWAI^{1,2,*} AND TAKU TSUCHIYA³

¹Department of Earth and Planetary Sciences, Tokyo Institute of Technology, Ookayama 2-12-1, Meguro, Tokyo 152-8551, Japan

²Department of Earth Science, University of California, Santa Barbara, California 93106, U.S.A.

³Geodynamics Research Center, Ehime University, Bunkyo-cho 2-5, Matsuyama, Ehime 790-8577, Japan

ABSTRACT

To understand the fate of the host phase for potassium subducted into the deep Earth's interior, we have studied the high-pressure stability and elastic properties of KAlSi_3O_8 hollandite (K-hollandite) by means of the first-principles computation method. Based on experimental observations, the tetragonal K-hollandite I phase was found to undergo a ferroelastic second-order phase transition to the monoclinic K-hollandite II phase at 14.9 GPa. This K-hollandite II phase was mechanically stable up to 150 GPa (i.e., entirely in the Earth's lower mantle), being consistent with previous studies. The Born's elastic stability criteria indicate that the tetragonal mechanical instability occurs at similar pressure of 16.9 GPa with shear softening. This causes anomalous pressure dependence of the wave velocities across the instability. Taking a Clapeyron slope of 7 MPa/K and a temperature of 1800 K, the transition pressure becomes ~28 GPa corresponding to about 770 km depth, which would be seismologically detectable and could be comparable to seismic scatterers observed at the shallowest lower mantle. Next, we studied the solid-solution effect of sodium to K-hollandite, indicating that it is very limited on the phase stability, although the Na-end-member phase was found to be metastable. Elasticity demonstrates strong anisotropy around 15 GPa due to its ferroelastic nature.

Keywords: Elastic property, phase transition, hollandite, first-principles, phase stability, anisotropy

INTRODUCTION

Long-lived radiogenic nuclides such as ^{40}K , ^{232}Th , ^{235}U , and ^{238}U are essential to understanding the Earth's long-term evolution, while short-lived such as ^{26}Al are important only for the very early Earth (Urey 1955). It is believed that these elements are distributed in the continental and oceanic crust and mantle and are concentrated especially in the continental crust. Since recent studies have demonstrated that continental crust can be subducted into the Earth's deep interior as well as a subducted slab despite of its buoyancy (Scholl and von Huene 2007; Kawai et al. 2009, 2012), it is important to understand the stability of the host phases of radiogenic nuclides such as ^{40}K .

Alkali feldspars in the KAlSi_3O_8 - $\text{NaAlSi}_3\text{O}_8$ system are the most abundant group of minerals in the Earth's crust. While alkali feldspars are minerals that can survive the initial stage of subduction, hollandite-type aluminosilicates with the large square tunnels formed by four double chains of edge-shared octahedra are a candidate for host phases of large elements and incompatible large-ion lithophile elements (LILEs) such as Rb, Ba Sr, K, Pb, La, Ce, and Th in the deep mantle. It is, therefore, essential to investigate stability and elasticity of hollandite in the Earth's deep interior.

Potassium feldspar is one of the most abundant minerals in the continental crust. Previous experimental studies on host phases of potassium show that KAlSi_3O_8 feldspar dissociates into an as-

semblage of $\text{K}_2\text{Si}_4\text{O}_9$ wadeite, Al_2SiO_5 kyanite, and SiO_2 coesite at 6–7 GPa and 1500 K, and the three phases further recombine into KAlSi_3O_8 hollandite (hereafter called as K-hollandite I) at about 9 GPa and 1500 K (Urakawa et al. 1994; Yagi et al. 1994). While experiments on K-rich alkali basalt using multi-anvil cell implied a phase transition of K-hollandite I at 22.5 GPa and 2000 K because quenched K-hollandite became Na- and Ca-richer (Wang and Takahashi 1999), some reported that K-hollandite I remains stable in the pressures range between 20 and 95 GPa at 900 K (Tutti et al. 2001). On the other hand, a new high-pressure $I2/m$ monoclinic structure of KAlSi_3O_8 (K-hollandite II) from an $I4/m$ tetragonal structure at 22 GPa and room temperature was confirmed by in situ X-ray diffraction measurements (Sueda et al. 2004). Later, the phase transition was suggested to be second-order (ferroelastic) because of marginal volume change during high-pressure studies up to 32 GPa and room temperature (Ferroir et al. 2006). The stability of K-hollandite II was investigated up to 128 GPa (Hirao et al. 2008). In contrast to the phase stability, the elasticities of the K-hollandite I and II phases were studied by theoretical studies (Mookherjee and Steinle-Neumann 2009). However, these previous studies are controversial both in terms of the reported phase transition pressure and elasticity. Some studies reported a second-order phase transition pressure of about 23 GPa (Caracas and Boffa Ballaran 2010; Deng et al. 2011), while the other suggested a first-order phase transition of 33 GPa (Mookherjee and Steinle-Neumann 2009). As for elasticity, one reported that the K-hollandite I phase becomes mechanically

* E-mail: kenji@geo.titech.ac.jp

unstable at 50 GPa (Mookherjee and Steinle-Neumann 2009), while another suggested a pressure of about 22 and 23 GPa (Caracas and Boffa Ballaran 2010; Deng et al. 2011).

While hollandite is the host phase for large elements such as LILEs, potassium could be replaced by sodium (Wang and Takahashi 1999). $K_{0.8}Na_{0.2}AlSi_3O_8$ hollandite I was reported to undergo a phase transition to hollandite II at 17–18 GPa (Boffa Ballaran et al. 2009). Then, $K_{0.8}Na_{0.2}AlSi_3O_8$ and $KAlSi_3O_8$ hollandite were theoretically predicted to undergo phase transitions at 13 and 23 GPa, respectively, suggesting that the solid-solution effect of sodium to K-hollandite be significant (Caracas and Boffa Ballaran 2010). The high-pressure behavior of the end-member $NaAlSi_3O_8$ albite composition has also been debatable. While some diamond-anvil cell experiments reported that $NaAlSi_3O_8$ hollandite (Na-hollandite) could be stable at some pressure (Liu 1978; Tutti 2007), some multi-anvil experiments and theoretical studies suggested that Na-hollandite is a metastable phase (Yagi et al. 1994; Liu 2006; Akaogi et al. 2010; Deng et al. 2010). In this paper, we have studied the high-pressure stability and elasticity of the $KAlSi_3O_8$ hollandite, and the solid-solution behavior of sodium to K-hollandite by means of ab initio density functional computation methods.

CRYSTAL STRUCTURE MODELS

The $KAlSi_3O_8$ hollandite I phase has a tetragonal crystal structure with the space group $I4/m$, which has a large square tunnel formed by double chains of edge-shared (Al,Si) O_6 octahedra, and K resides in the tunnel (Fig. 1a) (Ringwood et al. 1967; Yamada et al. 1984). As the large square tunnels formed by four double chains supply a space for large-ion elements such as K, Ba, Sr, Na, and Pb, hollandite-type silicate are considered as a possible repository of large alkali elements, especially potassium, in the lower mantle. On the other hand, the K-hollandite II phase has a monoclinic crystal structure with the space group $I2/m$, which has a distorted square formed by four double chains (Sueda et al. 2004; Ferroir et al. 2006; Hirao et al. 2008; Mookherjee and Steinle-Neumann et al. 2009; Caracas and Boffa Ballaran 2010). There is, however, no experimentally formal description in the crystallographic literature for the K-hollandite II phase, while a theoretical study predicted the atomic positions satisfying the space group $I2/m$ monoclinic symmetry (Mookherjee and Steinle-Neumann et al. 2009).

The disorder in (Al,Si) O_6 octahedra only in a single unit cell breaks the tetragonal symmetry due to the limited size. While a previous calculation using a single unit cell with 26 atoms breaks the symmetry (Deng et al. 2011), we therefore consider three supercells to maintain the tetragonal symmetry (Figs. 1b–1d). First, a $1 \times 1 \times 2$ supercell consists of two layers of $K_2Al_2Si_6O_{16}$ along *c*-axis, where one layer is stacked along *c*-axis on another layer with a 90° rotation around the *c*-axis (Fig. 1b; model A). Next, a $2 \times 2 \times 1$ supercell consists of four cells of $K_2Al_2Si_6O_{16}$ in the *c*-plane, where one cell is adjacent to another cell with a 90° rotation around the *c*-axis (Fig. 1c; model B). Finally, a $2 \times 2 \times 2$ supercell consists of two layers of $K_8Al_8Si_{24}O_{64}$ model B, where one layer is stacked along the *c*-axis on another layer with a 90° rotation around the *c*-axis (Fig. 1d; model C). Although conventional unit cells for models A, B, and C include 52, 104, and 208 atoms, respectively, all the primitive unit cells include

52 atoms. Previous studies used a 104 atom $1 \times 1 \times 4$ supercell in computation (Mookherjee and Steinle-Neumann et al. 2009) but their supercell is exactly identical to our model A with translation symmetry (personal communication with M. Mookherjee), and it is quite unclear why they chose the reducible cell.

To investigate solid-solution effect of sodium, we consider five $1 \times 1 \times 2$ supercells (model A in Fig. 1b) with Na content of 25 (Figs. 2a–2b), 50 (Fig. 2c), 75 (Fig. 2d), and 100 (Fig. 2e) mol%. The disorder effects are taken into account for Na content of 25 mol%. We consider two configurations of Na. One maintains the tetragonal symmetry (Fig. 2a), while another breaks the symmetry (Fig. 2b).

FIRST-PRINCIPLES COMPUTATION DETAILS

Our first-principles calculations are based on the density functional theory (Hohenberg and Kohn 1964; Kohn and Sham 1965) within the local density approximation (LDA) (Ceperley and Alder 1980; Perdew and Zunger 1981). One electron wavefunction satisfying the Kohn-Sham equation describes an electronic ground state, which was expanded by using the plane wave basis set. Ionic core potentials were approximated based on the pseudopotential method, which were generated using the Vanderbilt's method (Vanderbilt 1990) for K, Na, and O and Troullier and Martins' methods (Troullier and Martins 1991) for Al and Si. The electric configurations included in these pseudopotentials are $3s^23p^64s^1$ for K, $2s^22p^63s^1$ for Na, $3s^23p^1$ for Al, $3s^23p^3d^0$ for Si, and $2s^22p^4$ for O. Most of these have been well tested in our previous studies (Tsuchiya et al. 2004a, 2004b, 2005; Kawai and Tsuchiya 2010, 2012a, 2012b). The plane wave energy cutoff was set to 50 Ry, and the irreducible part of Brillouin zone was sampled on $2 \times 2 \times 2$ for the supercells of the K-hollandite I and II phases (52 atoms as mentioned above) using the Monkhorst-Pack method (Monkhorst and Pack 1976). Effects of using the larger cutoff and k-points on the calculated properties were found insignificant. The full elastic constant tensors of the class $4/m$ tetragonal and $2/m$ monoclinic structures have 7 and 13 independent components, respectively. They were calculated using the stress-strain relation with applying strains of ± 0.01 (Kawai and Tsuchiya 2010, 2012a, 2012b; Karki et al. 2001; Tsuchiya et al. 2004a, 2004b). We confirmed that the linear relation was ensured enough for this strain range. All structural parameters were fully relaxed to a static (0 K) configuration using the damped variable cell shape constant pressure molecular dynamics technique (Wentzcovitch 1991) using the PWSCF code (Giannozzi et al. 2009) until residual forces became less than 5.0×10^{-5} Ry/a.u. Computations for the K-hollandite II were performed from the structure, which was initially distorted in the *c*-plane until the structure was fully relaxed.

RESULTS AND DISCUSSION

To investigate the phase stability we calculated enthalpy for each supercell model for both K-hollandite I and II phases (Fig. 3a). We found that model A is the most stable, model C is the second for both K-hollandite I and II phases, although the enthalpy difference between model A and C is little. The supercells were found to have an enthalpy difference of about 30 kJ/mol between model A and B, which is produced clearly due to the difference in the configurations of Si/Al. Silicon

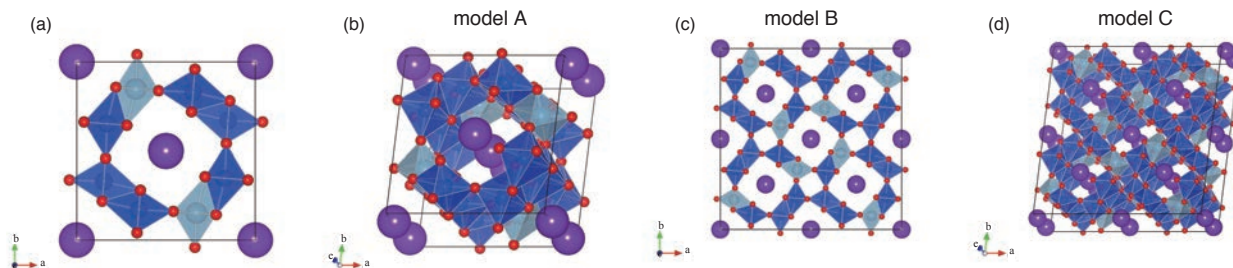


FIGURE 1. (a) Crystal structures of the KAlSi_3O_8 hollandite phases. Deep purple, light blue, dark blue, and red spheres represent K, Al, Si, and O atoms, respectively. (b) $1 \times 1 \times 2$ tetragonal supercell (model A), (c) $2 \times 2 \times 1$ tetragonal supercell (model B), and (d) $2 \times 2 \times 2$ tetragonal supercell (model C). (See supplemental data¹ for details of atomic positions for each model.) (Color online.)

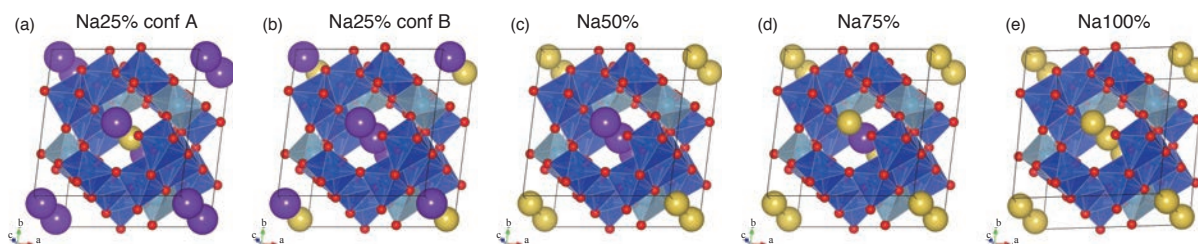


FIGURE 2. (a) Crystal structures of the $(\text{K,Na})\text{AlSi}_3\text{O}_8$ hollandite phases. Deep purple, yellow, light blue, dark blue, and red spheres represent K, Na, Al, Si, and O atoms, respectively. $1 \times 1 \times 2$ supercell with Na content of 25 mol% with (a; conf A) and without (conf B) the tetragonal symmetry. $1 \times 1 \times 2$ supercell with Na content of 50 (c), 75 (d), and 100 (e) mol% with tetragonal symmetry. (See supplemental data¹ for details of atomic positions for each model.) (Color online.)

and aluminum locally generate positive and negative charges, respectively. While Si is fairly randomly distributed in model A, Al is aligned both in the *c*-plane and along the *c*-axis in the cell shown in model B. This causes an enthalpy difference between model A and B. It is a little surprising that model C is about 3 kJ/mol more unstable than model A because model C is more symmetric than model A. Hence, in this study we consider model A to be the K-hollandite phase.

Next, we investigated the phase stability between the K-hollandite I and II phases. The enthalpy of K-hollandite II phase deviates from that of K-hollandite I phase at about 15 GPa and becomes lower than that of K-hollandite I phase above this pressure. The enthalpies for the K-hollandite I and II phases asymptotically converge at about 15 GPa with decreasing pressure. This kind of behavior is a typical feature for a second-order phase transition, which is likely expected to have a positive Clapeyron slope. If extrapolating experimental phase boundaries with a positive slope of ~ 7 MPa/K (Nishiyama et al. 2005; Ferroir et al. 2006), we obtain phase transition pressures of 16–18 GPa at static temperature. This pressure is consistent with our results. On the other hand, a previous theoretical study (Mookherjee and Steinle-Neumann 2009) reports that enthalpies for the K-hollandite I and II phases cross over one another at about 33 GPa, indicating a typical feature for a first-order phase

transition, even though the asymptotic feature can be seen in their enthalpy of the K-hollandite II phase around 20 GPa. They seem to have failed in computation of the reference structure of the K-hollandite I phase. Meanwhile, a previous theoretical study determined the transition pressure to be 23 GPa without any consideration of enthalpy difference between the K-hollandite I and II phases (Deng et al. 2011).

Pressure-volume relations calculated for the K-hollandite I and II phases are shown in Figure 4. Their equations of state parameters (zero-pressure bulk modulus, B_0 , and its pressure derivative, B'_0) determined by least-squares fitting to the third-order Birch-Murnaghan equation (Table 1) are $B_0 = 205.07$ GPa and $B'_0 = 4.18$ for the K-hollandite I phase and $B_0 = 192.26$ GPa and $B'_0 = 4.16$ for the K-hollandite II phase. We can obtain good agreement with experimental data for the K-hollandite I phase (Ferroir et al. 2006; Nishiyama et al. 2005; Zhang et al. 1993), although our computed volume for the K-hollandite I phase is about 1.4% smaller than experimental results due to no thermal effect for a static condition (Fig. 4 and Table 1). The K-hollandite II is more compressible than the K-hollandite I phase. Zero-pressure volume obtained by the recent calculations within the generalized gradient approximation (GGA) (Deng et al. 2011) is larger than that computed in this study within LDA as usually seen. While the zero-pressure volumes obtained in this study for both K-hollandite I and II phases match well with each other, a previous theoretical study shows difference in zero-pressure volumes between K-hollandite I and II phases (Mookherjee and Steinle-Neumann 2009), indicating that their computation is shy of convergence.

Computed lattice parameters for the K-hollandite I and II

¹ Deposit item AM-13-021, CIFs. Deposit items are available two ways: For a paper copy contact the Business Office of the Mineralogical Society of America (see inside front cover of recent issue) for price information. For an electronic copy visit the MSA web site at <http://www.minsocam.org>, go to the *American Mineralogist* Contents, find the table of contents for the specific volume/issue wanted, and then click on the deposit link there.

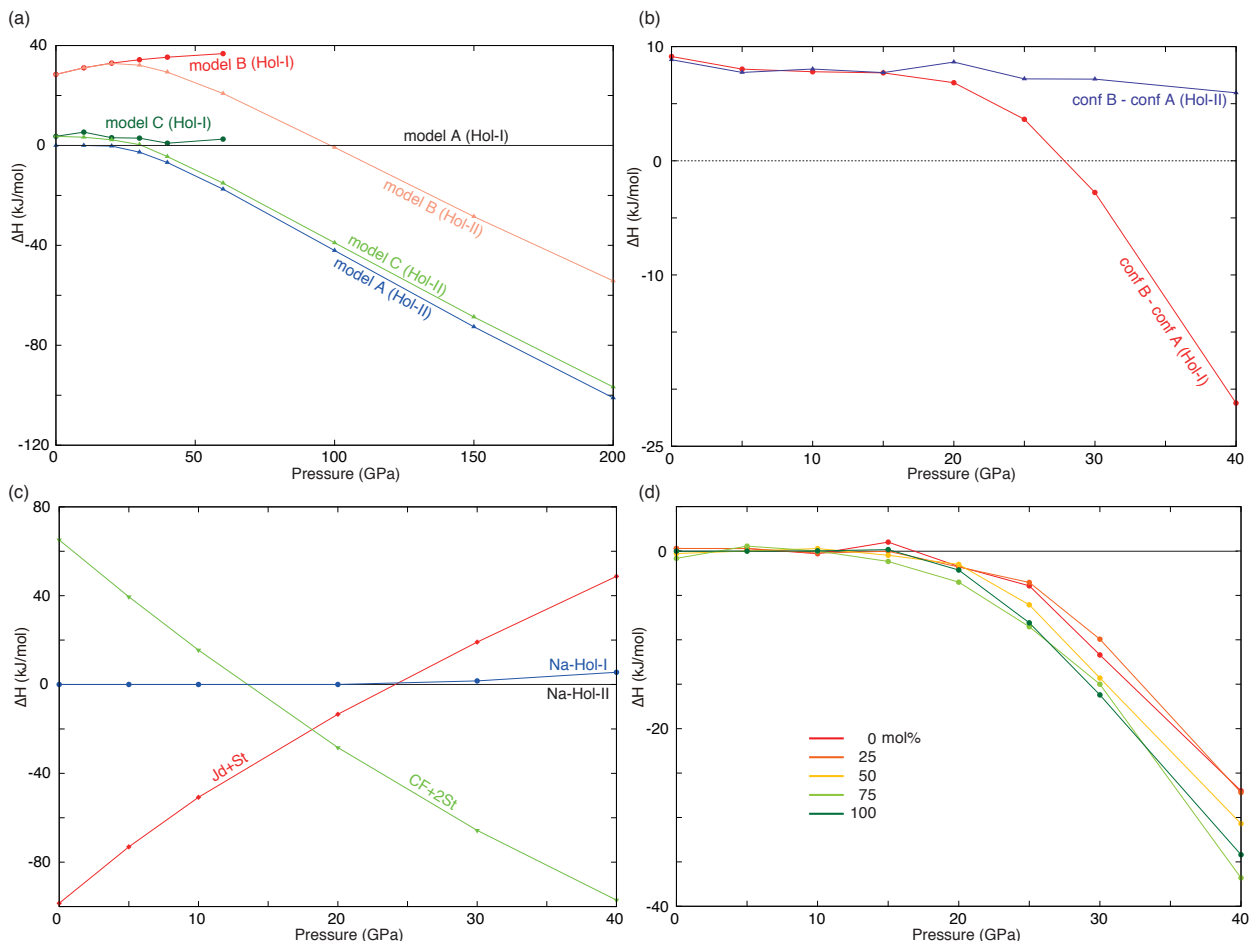


FIGURE 3. (a) The calculated enthalpy difference of the K-hollandite I and II phases for three supercell models relative to model A of the K-hollandite I phase (see Fig. 1). The phase transition pressure from K-hollandite I to II is determined to be 14.9 GPa by fitting the cell angle γ (see text for details). (b) The calculated enthalpy differences of the hollandite with Na content of 25 mol% and tetragonal conf A (red) and between conf B and monoclinic conf A (blue). (c) The enthalpy differences among an assemblage of jadeite ($\text{NaAlSi}_3\text{O}_6$) and stishovite (SiO_2), an assemblage of a CF-type phase (NaAlSiO_4) and stishovite (2SiO_2), and $\text{NaAlSi}_3\text{O}_8$ hollandite I and II. The enthalpy of hollandite II is taken as a reference. (d) The enthalpy differences of the K-hollandite I and II phases with Na content of 0, 25, 50, 75, and 100 mol% relative to K-hollandite I phase with each Na content. (Color online.)

phases are shown in Figure 5 as a function of pressure. These are in excellent agreement with the experimental data for both the K-hollandite I (Ferroir et al. 2006; Zhang et al. 1993) and II (Sueda et al. 2004; Ferroir et al. 2006; Hirao et al. 2008) phases. Although the bulk volume compressibility does not differ significantly between the K-hollandite I and II phases (Fig. 4), the splitting of cell parameters (a and b) and the change of the angle γ start rapidly at 20 GPa. The mean value $(a+b)/2$ and c do not change rapidly after the phase transition as reported by experimental studies (Ferroir et al. 2006; Hirao et al. 2008). Second-order phase transitions are critical phenomena. When we take a cell angle related to the monoclinic distortion, γ , as an order parameter, it can be described based on the Landau theory (Landau and Lifshitz 1994) as $\gamma \sim [(P - P_c)/P_c]^q$, where P_c and q are the critical pressure and the critical exponent related to the long-range order in the system, respectively. Calculated pressure variation in γ was well fitted by this formula in the pressure

range from 15 and 40 GPa and to provide $P_c = 14.9$ GPa and $q = 0.463$ (inset of Fig. 5c). This critical exponent is found close to the ideal value for classical second-order transitions of $1/2$.

Elastic constants of the K-hollandite I and II phases calculated are shown in Figure 6 as a function of pressure from 0 to 150 GPa and Table 2. Elastic constants of K-hollandite I and II are almost the same up to 10 GPa. Note that the relation $C_{16} = -C_{26}$ is satisfied in the class $4/m$ tetragonal structure (Nye 1985). This relation between the K-hollandite I and II phases is seen for the monoclinic K-hollandite II below 10 GPa, indicating that the monoclinic K-hollandite II spontaneously becomes tetragonal with decrease in pressure. In contrast, the softening in C_{11} and C_{66} of the tetragonal K-hollandite I phase occurs with increasing pressure over 40 GPa. This is consistent with previous theoretical studies (Mookherjee and Steinle-Neumann 2009; Caracas and Boffa Ballaran 2010).

For $1 \leq k \leq n$, the k -th principal submatrix of matrix **A** is

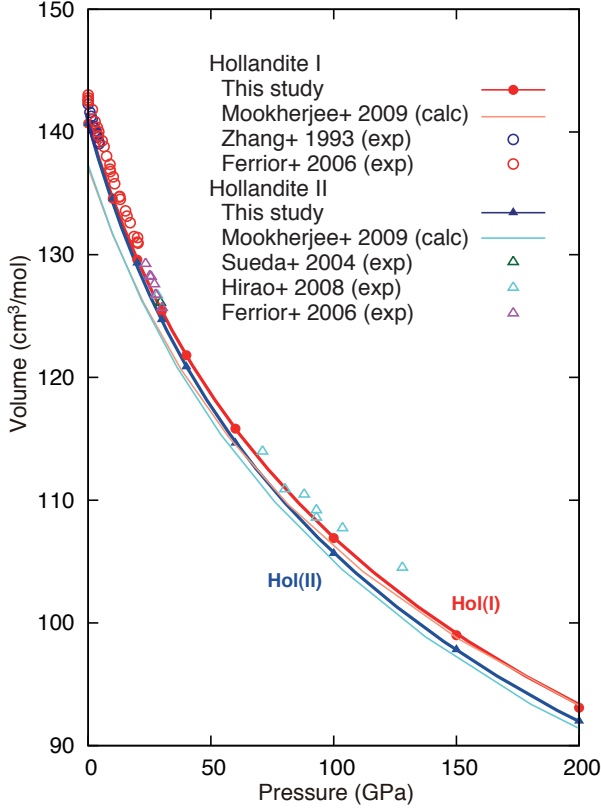


FIGURE 4. Volumes calculated for model A in Figure 2b of the K-hollandite I (circles) and II (triangles) phases. Fitting curves are computed using a third-order Birch-Murnaghan equation of state. We also show experimental results for the K-hollandite I (circles) (Ferroir et al. 2006; Zhang et al. 1993) and II (triangles) (Sueda et al. 2004; Ferroir et al. 2006; Hirao et al. 2008) in addition to theoretical results by Mookherjee and Steinle-Neumann (2009). (Color online.)

the $k \times k$ submatrix formed from the first k rows and first k columns of matrix \mathbf{A} . Its determinant is called as the (leading) k -th principal minor (Gilbert 1991). From Sylvester's criterion, a real, symmetric matrix is positive definite if and only if all its principle minors are positive. Since the energy density must be positive definite quadratic form (Born and Huang 1954), all the six (leading) principal minors of elastic tensor \mathbf{C} should be positive. For the class $4/m$ tetragonal structure, principal minors are as follows:

$$\begin{aligned}
 C(6) &= C_{66}, \\
 C(5, 6) &= C_{44}C_{66}, \\
 C(4, 5, 6) &= C_{44}^2C_{66}, \\
 C(3, 4, 5, 6) &= C_{33}C_{44}^2C_{66}, \\
 C(2, 3, 4, 5) &= (C_{11}C_{33}C_{66} - C_{13}^2C_{66} - C_{16}^2C_{33})C_{44}^2 \\
 C(1, 2, 3, 4, 5, 6) &= [(C_{11} - C_{12})C_{33}C_{66} - 2(C_{11} - C_{12})C_{13}^2C_{66} + 4C_{13}^2C_{16}^2 \\
 &\quad - 2\{(C_{11} + C_{12})C_{33} - 2C_{13}^2\}C_{16}^2]C_{44}^2
 \end{aligned} \tag{1}$$

TABLE 1. Equation of state parameters for the K-hollandite I and II phases calculated at the static temperature

	V_0 (cm ³ /mol)	B_0 (GPa)	B'_0
Hollandite-I (calc)*	140.70	205.07	4.18
Hollandite-I (calc)†	137.09	225.0	4.3
Hollandite-I (calc)‡	147.43	174.0	3.99
Hollandite-I (exp)§	142.3	180	4.0
Hollandite-I (exp)	143.1	183	4.0
Hollandite-I (exp)#	142.7	201	4.0
Hollandite-II (calc)*	140.7	192	4.16
Hollandite-II (calc)†	137.3	221	3.9
Hollandite-II (calc)‡	147.4	168	4.0

Notes: Results of previous theoretical and experimental studies are also shown. * This study. † Mookherjee and Steinle-Neumann (2009). ‡ Deng et al. (2011). § Zhang et al. (1993). || Nishiyama et al. (2005). # Ferroir et al. (2006).

We computed all the values and found $C(1,2,3,4,5,6)$ to be the mechanical stability condition for the tetragonal K-hollandite I phase. Hence, we computed a principal minor, $C(1,2,3,4,5,6)$, in the pressure from 0 to 60 GPa and found that the mechanical instability occurs around 16.9 GPa (Fig. 7a).

The class $4/m$ tetragonal symmetry with seven independent elastic constants is also known as $4/m$ (TII) Laue symmetry (Farley et al. 1975; Blanchfield et al. 1982). When the components of the elastic tensor of a $4/m$ (TII) Laue symmetry crystal are transformed by rotation around c -axis through an angle

$$\phi = \frac{1}{4} \tan^{-1} \left(\frac{4C_{16}}{C_{11} - C_{12} - 2C_{66}} \right) \tag{2}$$

then the transformed elastic constant C'_{16} becomes zero, the number of independent elastic constants is reduced from 7 to 6 and the elastic constant tensor C'_i makes the form of that of a $4/mmm$ (TI) Laue symmetry crystal. For elasticity tensor to be positive definite, the requirements obtained in the same manners as noted above are as follows:

$$C_{11} - C_{12} > 0, (C_{11} + C_{12})C_{33} - 2C_{13}^2 > 0, C_{44} > 0, \text{ and } C_{66} > 0 \tag{3}$$

Since $C_{11} - C_{12} > 0$ corresponds to the stability criterion for tetragonal stability for K-hollandite I phase, we found that the mechanical instability occurs 16.9 GPa (Fig. 7b), which is equal to the above computed results. This is of course quite reasonable because this rotational transformation operation is just algebraic and should not affect the elasticity of material itself.

Previous theoretical study (Caracas and Boffa Ballaran 2010) shows that $C_{66} < 0$ instead of $C_{11} - C_{12} < 0$ in Equation 3, but we did not confirm $C_{66} < 0$ even using the values reported in their paper. Instead, we found using their data tetragonal instability of $C_{11} - C_{12} < 0$ at about 31 GPa for a $4/m$ (TII) Laue symmetry crystal with six independent elastic constants and also found $C(1,2,3,4,5,6)$ in Equation 1 negative at almost the same pressure as 31 GPa even for a $4/mmm$ (TI) Laue symmetry crystal with seven independent elastic constants, although their data are too sparse in pressure to determine the critical pressure accurately. The difference in critical pressures may depend on their adopted method. They use the virtual crystal approximation, as it is called as *alchemical* approximation, for the Al/Si disordered sites. This approximation allows us to reduce the cell size and, thereby, computational cost. On the other hand,

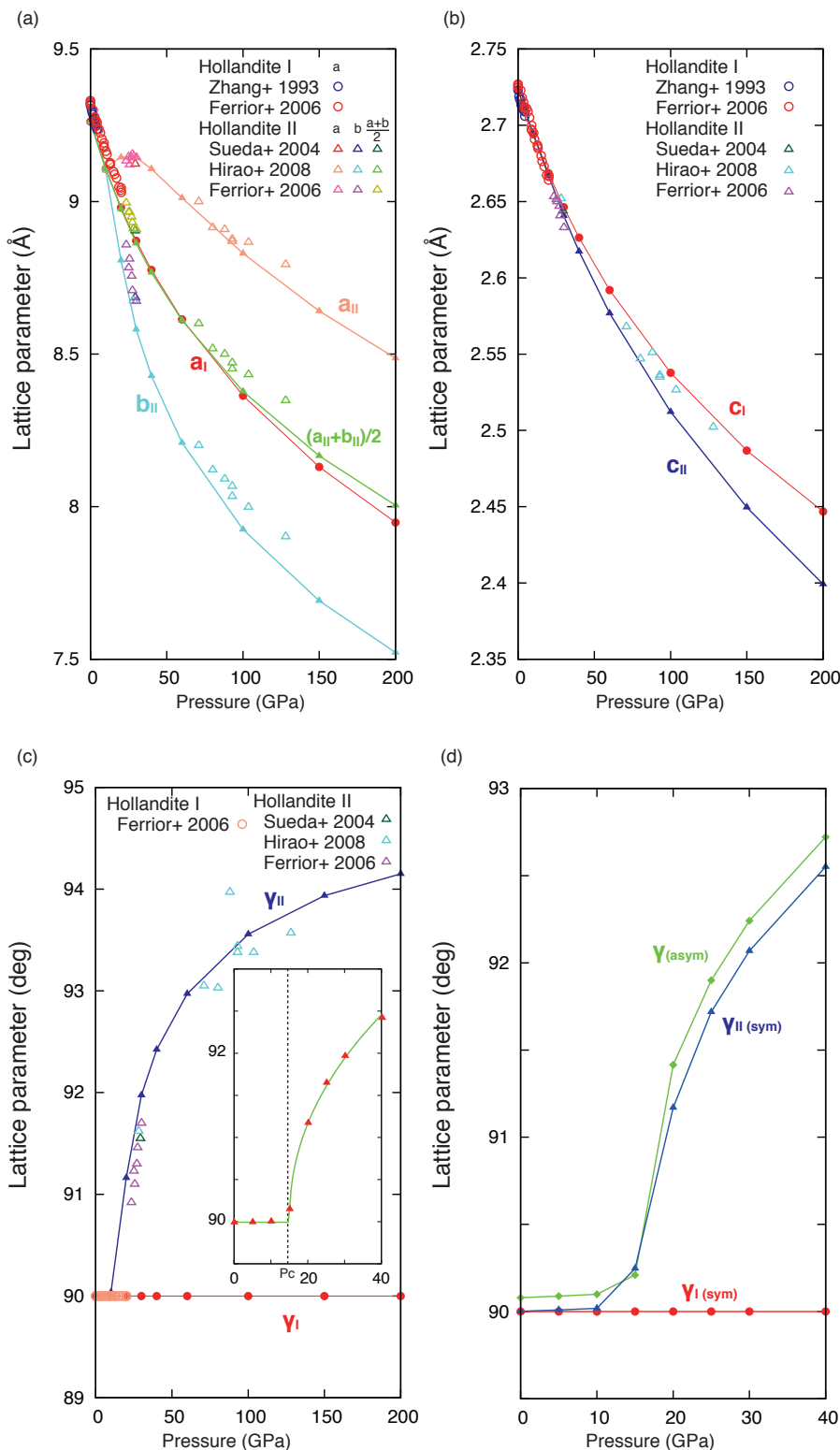


FIGURE 5. Lattice parameters (a and b in **a**; c in **b**; γ in **c**) calculated for model A of the K-hollandite I (circles) and II phases (triangles). We also show experimental results for the K-hollandite I (open circles) (Ferroir et al. 2006; Zhang et al. 1993) and II (open triangles) (Sueda et al. 2004; Ferroir et al. 2006; Hirao et al. 2008) phases. (inset of **c**) Calculated cell angle, γ (red triangle), with a fit (green line) (see text for details). (**d**) Calculated lattice parameters, γ , for K-hollandite I (red line) and II phases (blue line) with tetragonal symmetry and K-hollandite without tetragonal symmetry (green line) with Na content of 25 mol%. (Color online.)

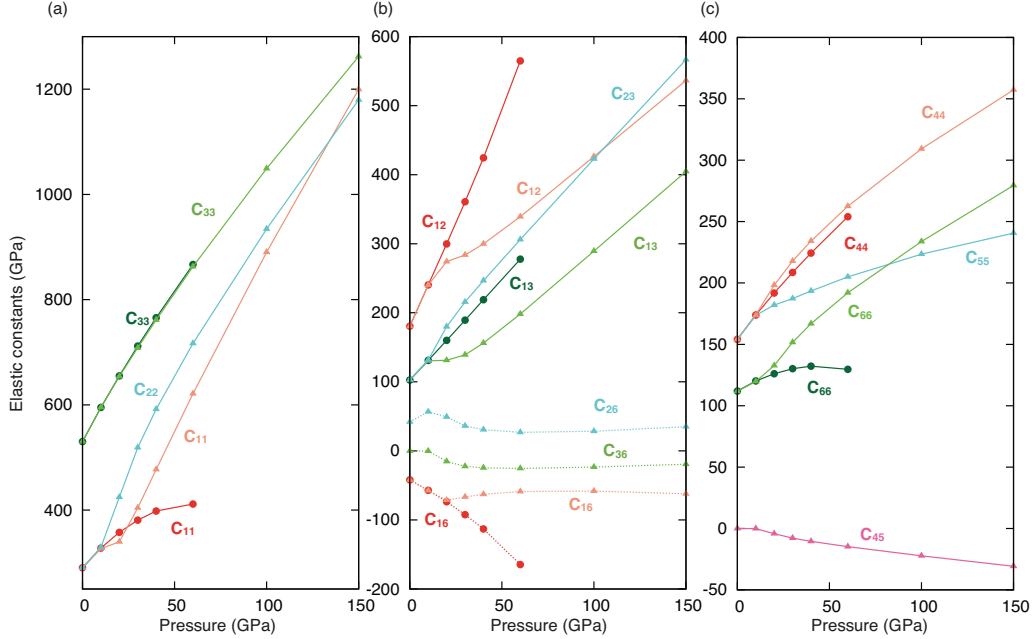


FIGURE 6. Elastic constants calculated as a function of pressure for model A of the K-hollandite I (0–60 GPa) and II (0–150 GPa) phases. (a–c) show longitudinal, off-diagonal, and shear components for the tetragonal K-hollandite I and monoclinic K-hollandite II phases. (Color online.)

TABLE 2. Elastic constants (C_{ij}), aggregate bulk (B), and shear (G) moduli of the K-hollandite I and II phases calculated at 0 GPa

	Hollandite-I (This study)	Hollandite-I* (This study)	Hollandite-I† (This study)	Hollandite-II (This study)	Hollandite-II* (This study)
C_{11} (GPa)	290	342	303	290	382
C_{22}	–	–	–	290	395
C_{33}	530	568	517	530	575
C_{44}	154	165	175	154	177
C_{55}	–	–	–	154	182
C_{66}	112	129	139	112	48
C_{12}	181	186	202	181	132
C_{13}	103	118	123	103	140
C_{23}	–	–	–	103	107
C_{16}	–42	–	44	–42	–16
C_{26}	–	–	–	42	4
C_{36}	–	–	–	–0.1	38
C_{45}	–	–	–	0.0	13
B	207	230	224	204	220
G	111	124	143 (117)‡	110	134
v_p (km/s)	9.46	9.87	10.19 (9.74)‡	9.45	9.92
v_s	5.28	5.53	5.98 (5.41)‡	5.28	5.75
v_ϕ	7.23	7.53	7.49	7.23	7.37

Notes: We also show results of previous theoretical studies.

* Mookherjee and Steinle-Neumann (2009).

† Caracas and Boffa Ballaran (2010).

‡ Recomputed using the data by Caracas and Boffa Ballaran (2010).

since *alchemical* pseudopotential for the disordered sites seems to make a crystal more symmetric, the K-hollandite I phase becomes more stable and the critical pressure increases. We suspect that an *alchemical* pseudopotential causes this discrepancy in the transition pressure (de Gironcoli and Baroni 1992).

Taking the Voigt-Reuss-Hill averages of the calculated elastic constants, we have obtained the isotropic bulk (B) and shear moduli (G), and isotropic compressional (v_p), shear (v_s), and bulk sound velocities (v_ϕ) of the both K-hollandite I and II phases as a function of pressure (Fig. 8). While no significant

anomaly is seen in the bulk modulus, a softening appears in the shear modulus associated with the K-hollandite I–II transition (Fig. 8b). The present calculations, therefore, show that the phase transition of K-hollandite I phase at 14.9 GPa produces the shear elastic instability (Fig. 8b).

Next, the single-crystal elastic wave velocities of both the K-hollandite I and II phases are calculated. Taking a Fourier transformation over space and time of the elastic equation of motion, we obtain Christoffel's equation:

$$\rho c^2 u_i = n_j n_l C_{ijkl} u_k \quad (4)$$

where ρ , c , and u are density, phase velocity and displacement vector, respectively and $(n_x, n_y, n_z) = (\sin\theta\cos\phi, \sin\theta\sin\phi, \cos\theta)$ is the direction cosine normal to wave surface. For Equation 4 to be satisfied, it is necessary that

$$\left| \rho c^2 \delta_{ik} - n_j n_l C_{ijkl} \right| = 0 \quad (5)$$

where δ_{ij} is the Kronecher's δ (Fryer and Frazer 1987). Solving this characteristic equation, we can obtain seismic velocities for three quasi-waves such as quasi-P, quasi-S1, and quasi-S2 waves because polarizations may not be along the dynamic axis. The azimuthal dependence of three phase velocities for the K-hollandite I phase at 0 and 20 GPa and the K-hollandite II phase at 20 and 100 GPa is shown in Figure 9. While we do not see changes of the anisotropic style, i.e., the fast and slow directions, for K-hollandite I phase between 0 and 20 GPa, quasi-S2 wave becomes very slow along [110] suggesting mechanical instability. The ϕ -dependence of the K-hollandite I and II phase has periods of 180° and 90° due to the difference

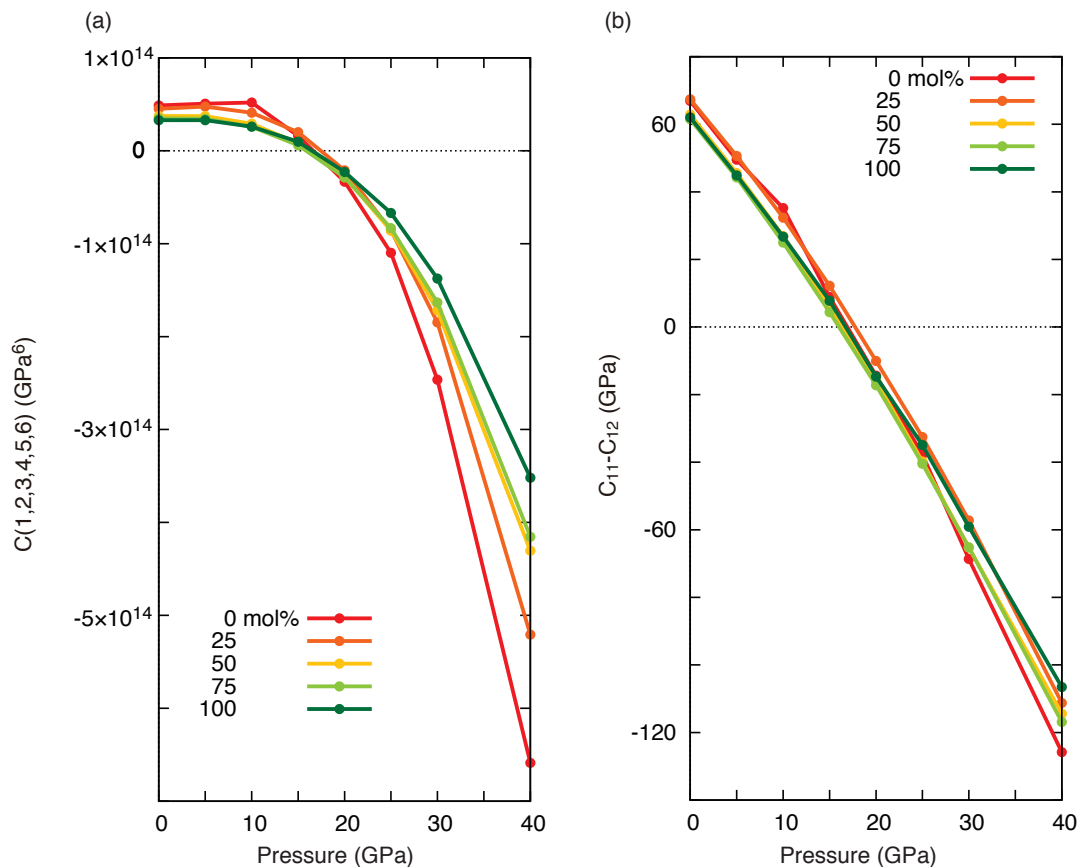


FIGURE 7. Mechanical stability criterion computed for the K-hollandite I phase with Na content of 0, 25, 50, 75, and 100 mol%. (a) $C(1,2,3,4,5,6)$ in Equation 1 for the class $4/m$ tetragonal structure. (b) $C_{11}-C_{12}$ in Equation 3 for the class $4/mmm$ tetragonal structure. (Color online.)

between tetragonal and monoclinic systems. The fast and slow directions, in particular for the S waves, change very much with pressure for the K-hollandite II phase, although the magnitude of anisotropy decreases with increasing pressure. Next we define the azimuthal anisotropy for the P and S waves as follows:

$$A_p = \frac{v_{p_{\max}} - v_{p_{\min}}}{v_p} \times 100; \quad A_s = \frac{v_{s_{\max}} - v_{s_{\min}}}{v_s} \times 100 \quad (6)$$

where v_p and v_s are the isotropic aggregate velocities (Fig. 7). The K-hollandite becomes strongly anisotropic around 20 GPa (Fig. 10). In particular, the S wave anisotropy diverges. This clearly reflects the ferroelastic nature of the phase transition.

Finally, the solid-solution effect of sodium to K-hollandite is considered. To investigate the phase stability, we compute enthalpy for each symmetric supercell for Na content of 25 (Fig. 2a), 50 (Fig. 2c), 75 (Fig. 2d), 100 (Fig. 2e) mol% for both K-hollandite I and II phases (Fig. 3d). Significant solid-solution effects to phase stability cannot be found via enthalpy comparison. We also compute the mechanical stability conditions for each supercell and find that the instability occurs in the pressure range from 16 to 18 GPa for all the Na content (Fig. 7). This also suggests that the solid-solution effect is insignificant. This pressure is very consistent with previous

experimental results which reported that $K_{0.8}Na_{0.2}AlSi_3O_8$ hollandite undergoes a phase transition to hollandite II at 17–18 GPa (Boffa Ballaran et al. 2009). On the other hand, previous theoretical studies predicted that $K_{0.8}Na_{0.2}AlSi_3O_8$ and $KAlSi_3O_8$ hollandites undergo phase transitions at 13 and 23 GPa, respectively, and the solid-solution effect of sodium to K-hollandite is significant (Caracas and Boffa Ballaran 2010). As noted above, we suspect that *alchemical* pseudopotential causes this discrepancy in the transition pressure (de Gironcoli and Baroni 1992). We also compute enthalpy differences between $K_{0.75}Na_{0.25}AlSi_3O_8$ hollandite I and $KAlSi_3O_8$ hollandite I and between $K_{0.75}Na_{0.25}AlSi_3O_8$ hollandite II and $KAlSi_3O_8$ hollandite II. Since these values are coincident within 0.001 kJ/mol both before and after the phase transition. This suggests that the solid-solution effects of sodium to both K-hollandite I and II are almost the same in contrast to previous experimental results (Wang and Takahashi 1999). This may be caused by other effects such as the solid-solution effects of sodium to other phases in their sample.

Then, the disorder effect in (K,Na) in the tunnel (Figs. 2a–2b) is studied. Although the supercell without the tetragonal symmetry (Fig. 2b) becomes spontaneously strained with increasing pressure, this pressure of about 17 GPa is barely different from the pressure at which the supercell with the tetragonal symmetry (Fig. 2a) undergoes a phase transition

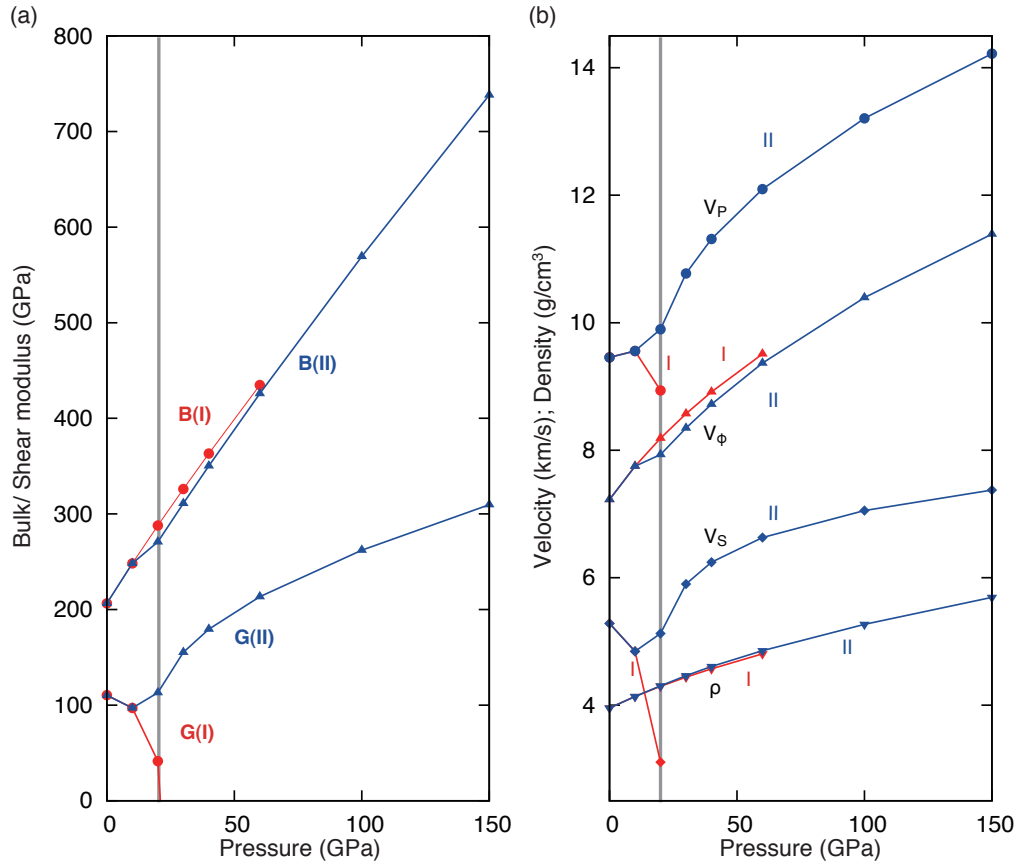


FIGURE 8. (a) Aggregate bulk and shear moduli of the K-hollandite I (red) and II (blue) phases. (b) Longitudinal, bulk and shear wave velocities and densities of the K-hollandite I and II phases. The vertical bold lines represent the calculated transition pressure of hollandites. (Color online.)

to monoclinic hollandite II (Fig. 3b). The supercell without the symmetry (Fig. 2b) is about 2.5 kJ/mol less stable than with the symmetry (Fig. 2a). Since this enthalpy difference is very small, both configurations with and without tetragonal configurations will be randomly distributed under high *P-T* condition in the mantle. To understand random configuration effects to the phase transition between K-hollandite I and II, we investigate the pressure dependence of a cell-parameter, γ , for configurations both with and without tetragonal symmetry (Fig. 5d). Although a configuration without tetragonal symmetry (green line) has a distorted structure in all the pressure range, the distortion is very small up to 15 GPa and γ without tetragonal symmetry increases in the same manner as that with tetragonal symmetry (blue line). This suggests that even for a configuration without tetragonal symmetry, the phase transition occurs at the same pressure as with tetragonal symmetry. Hence, random distribution of structure with and without tetragonal symmetry would not influence the phase transition pressure. Also, although it may be monoclinic locally, due to random distributions K-hollandite should be tetragonal up to the phase transition pressure.

Next, phase stability in NaAlSi₃O₈ system is considered. We calculate the enthalpy for an assemblage of jadeite (NaAlSi₂O₆) and stishovite (SiO₂), an assemblage of a CF-type phase (NaAlSiO₄) and stishovite (2SiO₂), and NaAlSi₃O₈ hollandite

I and II, and have found that an assemblage of jadeite and stishovite is stable up to 18 GPa and an assemblage of a CF-type phase and stishovite is stable over 18 GPa. This is consistent with previous theoretical studies (Deng et al. 2010; Kawai and Tsuchiya 2010, 2012c), although the transition pressure of 18 GPa (Kawai and Tsuchiya 2010, 2012c) is different from that of 33.6 GPa (Deng et al. 2010). The former matches well with experimental results (Akaogi et al. 2010). Our calculation suggests that the Na-hollandite is a metastable phase as previous studies noted.

GEOPHYSICAL IMPLICATIONS

Sediment and Archaean granites become less dense near the Earth's surface but contain about 20 vol% of the K-hollandite I phase above 9 GPa during subduction in the upper mantle, respectively (Irifune et al. 1994; Wu et al. 2009). Taking temperatures of 1300 (cold geotherm) and 1800 K (normal geotherm) and pressures around the boundary between upper and lower mantles into account, the mechanical instability (Fig. 7b) of the K-hollandite I occurs at 24.8 and 28.3 GPa, with a Clapeyron slope of 7 MPa/K (Nishiyama et al. 2005), corresponding to the depth of 692 and 771 km, respectively. In the depth range between the depth at which mechanical stability starts and the depth at which phase transition is completed, the velocity changes due to both softening of shear modulus

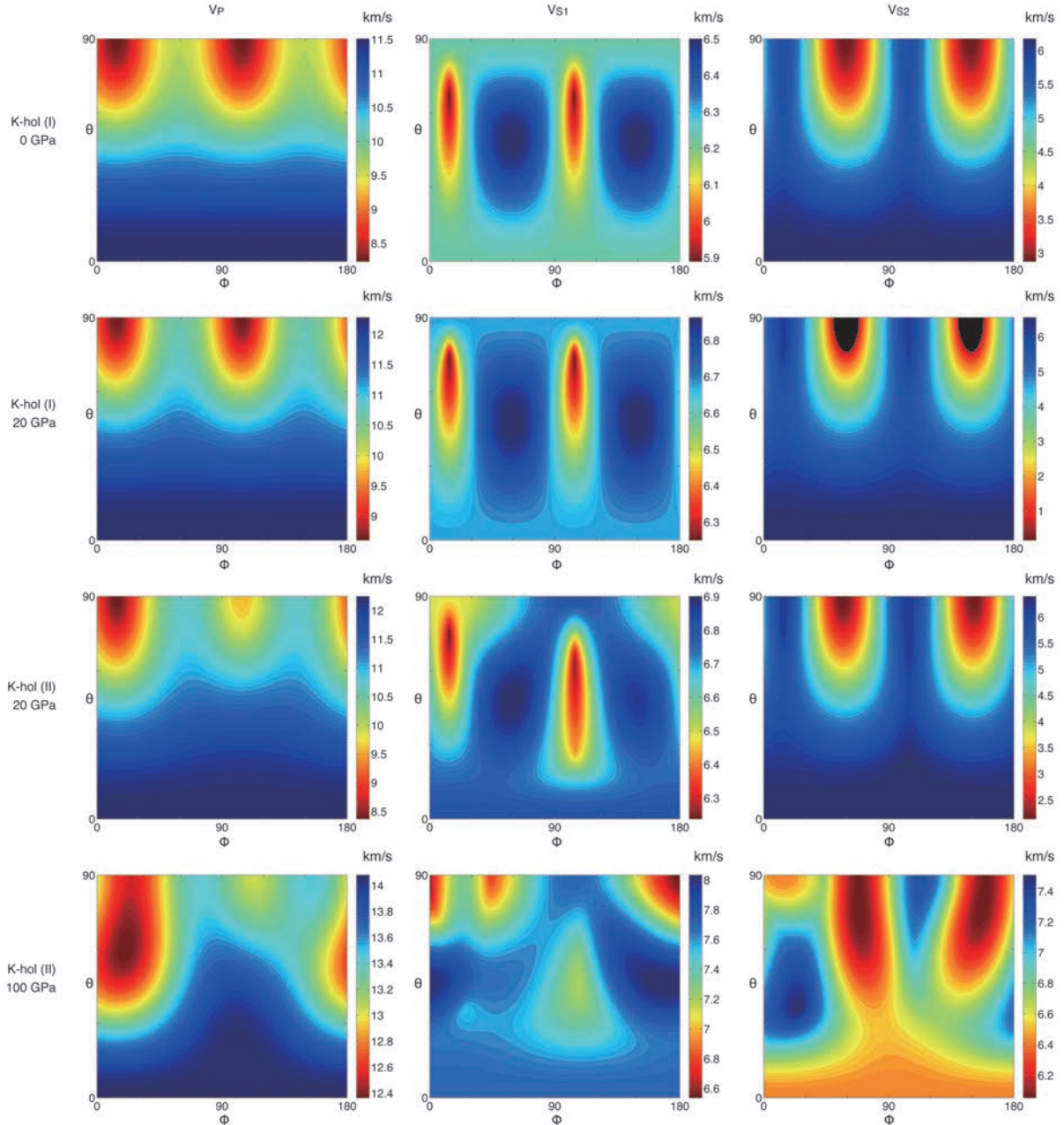


FIGURE 9. Velocities of quasi-waves (qV_p , qV_{S1} , and qV_{S2}), where $qS1$ is the faster of the two split shear waves, as a function of the propagation direction for the K-hollandite I phase at 0 and 20 GPa and the K-hollandite II phase at 20 and 100 GPa. (Color online.)

of the K-hollandite I phase and phase transition between the K-hollandite I and II phase can be observed. This is consistent with evidence on the seismic scatterers observed in the shallowest lower mantle (Kaneshima 2009), suggesting that buoyant granitic material can be subducted into the deep mantle and be carried to another gravitationally stable depth range other than the Earth's surface (Kawai et al. 2009, 2012).

Since the K-hollandite is stable entirely in the lower mantle, they can be a host phase for large elements in the Earth's deep interior. The K-hollandite controls a significant proportion of the whole-rock budget of incompatible elements. Recycling of con-

tinental sediments including the K-hollandite subducted into the mantle transition zone can explain the geochemical trace element abundance in EM-I type ocean-island basalts (Rapp et al. 2008). Also, geochemical studies on potassium-rich lamproites from Gausberg, Antarctica (Murphy et al. 2002) suggested that the source of lamproites should be effectively isolated for 2–3 Gyr in the mantle. Since the granitic materials including the K-hollandite are gravitationally stable in the mantle transition zone (Kawai et al. 2009), the mantle transition zone could be reservoir of incompatible LILEs, solving the terrestrial Pb-isotope paradox (Murphy et al. 2002; Kawai et al. 2010, 2012).

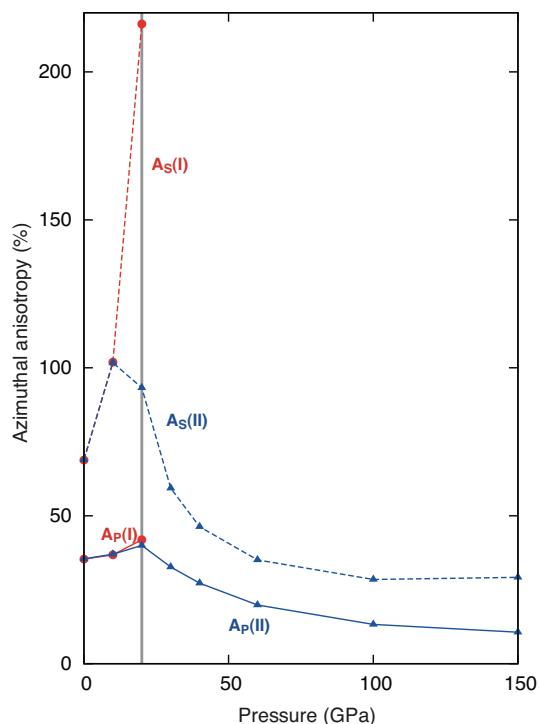


FIGURE 10. Pressure dependence of the elastic anisotropy of the K-hollandite I and II phases. (Color online.)

ACKNOWLEDGMENTS

We thank Haruhiko Dekura and Shinji Yamamoto for valuable discussions, and also thank Mainak Mookherjee for providing the atomic positions of K-hollandite. This work was completed under the supports by JSPS Fellowships for Young Scientists and KAKENHI (Grand No. 24840020) to K.K., in part by KAKENHI (Grant No. 23540560) to T.T., and by Ehime University Global Centers of Excellence program “Deep Earth Mineralogy”.

REFERENCES CITED

- Akaogi, M., Haraguchi, M., Nakanishi, K., Ajiro, H., and Kojitani, H. (2010) High-pressure phase relations in the system $\text{CaAl}_4\text{Si}_2\text{O}_{11}$ – $\text{NaAl}_3\text{Si}_3\text{O}_{11}$ with implication for Na-rich CAS phase in shocked Martian meteorites. *Earth and Planetary Science Letters*, 289, 503–508.
- Blanchfield, P., Saunders, G.A., and Hailing, T. (1982) The hydrostatic pressure derivatives of the elastic constants of the scheelites LiYF_4 and $\text{LiY}_{0.5}\text{Tb}_{0.5}\text{F}_4$. *Journal of Physics C: Solid State Physics*, 15, 2081–2092.
- Boffa Ballaran, T., Liu, J., Dubrovinsky, L.S., Caracas, R., and Crichton, W. (2009) High-pressure ferroelastic phase transition in aluminosilicate hollandite. *Physical Review B*, 80, 21404.
- Born M. and Huang, K. (1954) *Dynamical Theory of Crystal Lattices*. Oxford University Press, U.K.
- Caracas, R. and Boffa Ballaran, T. (2010) Elasticity of (K,Na)AlSi₃O₈ hollandite from lattice dynamics calculations, *Physics of the Earth and Planetary Interiors*, 181, 21–26.
- Ceperley, D. and Alder, B. (1980) Ground state of the electron gas by a stochastic method, *Physical Review Letters*, 45, 566–569.
- de Gironcoli, S. and Baroni, S. (1992) Effects of disorder on the vibrational properties of SiGe alloys: Failure of mean-field approximations. *Physical Review Letters*, 69, 1959–1962.
- Deng, L., Liu, X., Liu, H., and Dong, J. (2010) High-pressure phase relations in the composition of albite $\text{NaAlSi}_3\text{O}_8$ constrained by an ab initio and quasi-harmonic Debye model, and their implications. *Earth and Planetary Science Letters*, 298, 427–433.
- Deng, L., Liu, X., Liu, H., and Zhang, Y. (2011) A first-principles study of the phase transition from Holl-I to Holl-II in the composition KAlSi_3O_8 . *American Mineralogist*, 96, 974–982.
- Farley, J.M., Saunders, G.A., and Chung, D.Y. (1975) Elastic properties of scheelite structure molybdates and tungstates. *Journal of Physics C: Solid State Physics*, 8, 780–786.
- Ferroir, T., Onozawa, T., Yagi, T., Merkel, S., Miyajima, N.H., Nishiyama, N., Irifune, T., and Kikegawa, T. (2006) Equation of state and phase transition in KAlSi_3O_8 hollandite at high pressure. *American Mineralogist*, 91, 327–332.
- Fryer, G.J. and Frazer, L.N. (1987) Seismic waves in stratified anisotropic media – II. Elastodynamic eigensolutions for some anisotropic systems. *Geophysical Journal of the Royal Astronomical Society*, 91, 73–101.
- Giannozzi, P., Baroni, S., Bonini, N., Calandra, M., Car, R., Cavazzoni, C., Ceresoli, D., Chiarotti, G.L., Cococcioni, M., Dabo, I., and others. (2009) QUANTUM ESPRESSO: A modular and open-source software project for quantum simulations of materials. *Journal of Physics: Condensed Matter*, 21, 395502–395521.
- Gilbert, G.T. (1991) Positive definite matrices and Sylvester’s criterion. *The American Mathematical Monthly*, 98, 44–46.
- Hirao, N., Ohtani, E., Kondo, T., Sakai, T., and Kikegawa, T. (2008) Hollandite II phase in KAlSi_3O_8 as a potential host mineral of potassium in the Earth’s lower mantle. *Physics of the Earth and Planetary Interiors*, 166, 97–104.
- Hohenberg, P. and Kohn, W. (1964) Inhomogeneous electron gas. *Physical Review B*, 136, 864–871.
- Irifune, T., Ringwood, A.E., and Hibberson, W.O. (1994) Subduction of continental crust and terrigenous and pelagic sediments: an experimental study. *Earth and Planetary Science Letters*, 126, 351–368.
- Kaneshima, S. (2009) Seismic scatterers at the shallowest lower mantle beneath subducted slabs. *Earth and Planetary Science Letters*, 286, 304–315.
- Karki, B.B., Stixrude, L., and Wentzcovitch, R.M. (2001) High-pressure elastic properties of major materials of Earth’s mantle from first principles. *Reviews of Geophysics*, 39, 507–534, doi:10.1029/2000RG000088.
- Kawai, K. and Tsuchiya, T. (2010) Ab initio investigation of high-pressure phase relation and elasticity in the $\text{NaAlSi}_3\text{O}_8$ system. *Geophysical Research Letters*, 37, L17302, doi:10.1029/2010GL044310.
- (2012a) Phase stability and elastic properties of the NAL and CF phases in the $\text{NaMg}_2\text{Al}_5\text{SiO}_{12}$ system from first principles. *American Mineralogist*, 97, 305–314.
- (2012b) First principles investigations on the elasticity and phase stability of grossular garnet. *Journal of Geophysical Research*, 117, B02202, doi:10.1029/2011JB008529.
- (2012c) High-*P*, *T* phase relations in the $\text{NaAlSi}_3\text{O}_8$ system from first-principles computation. *Physics, and Chemistry of Minerals*, 39, 305–310.
- Kawai, K., Tsuchiya, T., Tsuchiya, J., and Maruyama, S. (2009) Lost primordial continents. *Gondwana Research*, 16, 581–586.
- Kawai, K., Tsuchiya, T., and Maruyama, S. (2010) The second continent. *Journal of Geography*, 119, 1197–1214.
- Kawai, K., Yamamoto, S., Tsuchiya, T., and Maruyama, S. (2012) The second continent: Existence of granitic continental materials around the bottom of the mantle transition zone. *Geoscience Frontiers*, in press, <http://dx.doi.org/10.1016/j.gsf.2012.08.003>.
- Kohn, W. and Sham, L.J. (1965) Self-consistent equations including exchange and correlation effects. *Physical Review A*, 140, 1133–1138.
- Landau, L.D. and Lifshitz, E.M. (1994) *Statistical Physics Part 2*, vol. 9 of *Course of Theoretical Physics*, 3rd ed. Pergamon, New York.
- Liu, L.G. (1978) High-pressure phase transformations of albite, jadeite and nepheline. *Earth and Planetary Science Letters*, 37, 438–444.
- Liu, X. (2006) Phase relations in the system KAlSi_3O_8 – $\text{NaAlSi}_3\text{O}_8$ at high pressure–high temperature conditions and their implication for the petrogenesis of lingunite. *Earth and Planetary Science Letters*, 246, 317–325.
- Monkhorst, H.J. and Pack, J.D. (1976) Special points for Brillouin-zone integrations. *Physical Review B*, 13, 5188–5192.
- Mookherjee, M. and Steinle-Neumann, G. (2009) Detecting deeply subducted crust from the elasticity of hollandite. *Earth and Planetary Science Letters*, 288, 349–358.
- Murphy, D.T., Collerson, K.D., and Kamber, B.S. (2002) Lamproites from Gaussberg, Antarctica: Possible transition zone melts of Archaean subducted sediments. *Journal of Petrology*, 43, 981–1001.
- Nishiyama, N., Rapp, R.P., Irifune, T., Sanehira, T., Yamazaki, D., and Funakoshi, K. (2005) Stability and P-V-T equation of state of KAlSi_3O_8 -hollandite determined by in situ X-ray observations and implications for dynamics of subducted continental crust material. *Physics and Chemistry of Minerals*, 32, 627–637.
- Nye, J.F. (1985) *Physical Properties of Crystals: Their Representation by Tensors and Matrices*. Oxford University Press, U.K.
- Perdew, J.P. and Zunger, A. (1981) Self-interaction correction to densityfunctional approximations for many-electron systems. *Physical Review B*, 23, 5048–5079.
- Rapp, R.P., Irifune, T., Shimizu, N., Nishiyama, N., Norman, M.D., and Inoue, T. (2008) Subduction recycling of continental sediments and the origin of geochemically enriched reservoirs in the deep mantle. *Earth and Planetary Science Letters*, 271, 14–23.
- Ringwood, A.E., Reid, A.F., and Wadsley, A.D. (1967) High-pressure KAlSi_3O_8 , an aluminosilicate with sixfold coordination. *Acta Crystallographica*, 23, 1093–1095.
- Scholl, D.W. and von Huene, R. (2007) Crustal recycling at modern subduction

- zones applied to the past. *Geological Society of America Memoirs*, 200, 9–32.
- Sueda, Y., Irifune, T., Nishiyama, N., Rapp, R.P., Ferroir, T., Onozawa, T., Yagi, T., Merkel, S., Miyajima, N., and Funakoshi, K. (2004) A new high-pressure form of KAlSi_3O_8 under lower mantle conditions. *Geophysical Research Letters*, 31, L23612, doi:10.1029/2004GL021156.
- Troullier, N. and Martins, J.L. (1991) Efficient pseudopotential for planewave calculations. *Physical Review B*, 43, 1993–2006.
- Tsuchiya, J., Tsuchiya, T., and Wentzcovitch, R.M. (2005) Transition from the $\text{Rh}_2\text{O}_3(\text{II})$ -to- CaIrO_3 structure and the high-pressure-temperature phase diagram of alumina. *Physical Review B*, 72, 020103(R).
- Tsuchiya, T., Tsuchiya, J., Umemoto, K., and Wentzcovitch, R.M. (2004a) Phase transition in MgSiO_3 perovskite in the Earth's lower mantle. *Earth and Planetary Science Letters*, 224, 241–248.
- (2004b) Elasticity of post-perovskite MgSiO_3 . *Geophysical Research Letters*, 31, L14603, doi:10.1029/2004GL020278.
- Tutti, F. (2007) Formation of end-member $\text{NaAlSi}_3\text{O}_8$ hollandite-type structure (lingunite) in diamond anvil cell. *Physics of the Earth and Planetary Interiors*, 161, 143–149.
- Tutti, F., Dubrovinsky, L.S., Saxena, S.K., and Carlson, S. (2001) Stability of KAlSi_3O_8 hollandite-type structure in the Earth's lower mantle conditions. *Geophysical Research*, 28, 2735.
- Urakawa, S., Kondo, T., Igawa, N., Shimomura, O., and Ohno, H. (1994) Synchrotron radiation study on the high-pressure and high-temperature phase relations of KAlSi_3O_8 . *Physics and Chemistry of Minerals*, 21, 387–391.
- Urey, H.C. (1955) The cosmic abundances of potassium, uranium, and thorium and the heat balances of the Earth, the Moon, and Mars. *Proceedings of the National Academy of Sciences*, 41, 127–144.
- Vanderbilt, D. (1990) Soft self-consistent pseudopotentials in a generalized eigenvalue formalism. *Physical Review B*, 41, 7892–7895.
- Wang, W. and Takahashi, E. (1999) Subsolidus and melting experiments of a K-rich basaltic composition to 27 GPa: Implication for the behavior of potassium in the mantle. *American Mineralogist*, 84, 357–361.
- Wentzcovitch, R.M. (1991) Invariant molecular dynamics approach to structural phase transitions. *Physical Review B*, 44, 2358–2361.
- Wu, Y., Fei, Y., Jin, Z., and Liu, X. (2009) The fate of subducted upper continental crust: An experimental study. *Earth and Planetary Science Letters*, 282, 275–284.
- Yagi, A., Suzuki, T., and Akaogi, M. (1994) High pressure transitions in the system KAlSi_3O_8 - $\text{NaAlSi}_3\text{O}_8$. *Physics and Chemistry of Minerals*, 21, 12–17.
- Yamada, H., Matsui, Y., and Ito, E. (1984) Crystal-chemical characterization of KAlSi_3O_8 with the hollandite structure. *Mineralogical Journal*, 12, 29–34.
- Zhang, J., Ko, J., Hazen, R.M., and Prewitt, C.T. (1993) High-pressure crystal chemistry of KAlSi_3O_8 hollandite. *American Mineralogist*, 78, 493–499.

MANUSCRIPT RECEIVED DECEMBER 7, 2011

MANUSCRIPT ACCEPTED AUGUST 15, 2012

MANUSCRIPT HANDLED BY BIJAYA KARKI